10722–10733 *Nucleic Acids Research, 2015, Vol. 43, No. 22* *Published online 9 September 2015*
doi: 10.1093/nar/gkv884

Effects of non-CpG site methylation on DNA thermal stability: a fluorescence study

Luca Nardo[1,*], Marco Lamperti[2], Domenico Salerno[1], Valeria Cassina[1], Natalia Missana[1], Maria Bondani[3], Alessia Tempestini[4] and Francesco Mantegazza[1]

[1]Department of Health Sciences, University of Milano Bicocca, Via Cadore 48, Monza, MB 20900, Italy, [2]Department of Science and High Technology, University of Insubria, Via Valleggio 11, Como, CO 22100, Italy, [3]Institute for Photonics and Nanotechnology, National Research Council, Via Valleggio 11, Como, CO 22100, Italy and [4]LENS-Department of Physics and Astronomy, University of Firenze, Via Sansone 1, Sesto Fiorentino, FI 50019, Italy

Received May 26, 2015; Revised August 05, 2015; Accepted August 21, 2015

ABSTRACT

Cytosine methylation is a widespread epigenetic regulation mechanism. In healthy mature cells, methylation occurs at CpG dinucleotides within promoters, where it primarily silences gene expression by modifying the binding affinity of transcription factors to the promoters. Conversely, a recent study showed that in stem cells and cancer cell precursors, methylation also occurs at non-CpG pairs and involves introns and even gene bodies. The epigenetic role of such methylations and the molecular mechanisms by which they induce gene regulation remain elusive. The topology of both physiological and aberrant non-CpG methylation patterns still has to be detailed and could be revealed by using the differential stability of the duplexes formed between site-specific oligonucleotide probes and the corresponding methylated regions of genomic DNA. Here, we present a systematic study of the thermal stability of a DNA oligonucleotide sequence as a function of the number and position of non-CpG methylation sites. The melting temperatures were determined by monitoring the fluorescence of donor-acceptor dual-labelled oligonucleotides at various temperatures. An empirical model that estimates the methylation-induced variations in the standard values of hybridization entropy and enthalpy was developed.

INTRODUCTION

Cytosine methylation is possibly the most widespread epigenetic marker in the genomes of eukaryotes, ranging from fungi and plants to animals, including mammals and humans. Forty years have passed since two seminal papers were published in 1975 (1,2) and independently suggested that cytosine methylation could act as a stably inherited modification that affects gene regulation and cellular differentiation. In these papers, particular care was already devoted to the study of the methylation occurring at the CpG dinucleotides within CpG islands (CGIs). CGIs are relatively short (≈1 kb) sequences that are notably enriched in CpGs and mainly occur within gene promoters (GPs), typically at or next to transcription start sites (TSSs). The cytosine methylation at these sites systematically inhibits the binding of the DNA-binding proteins responsible for transcription initiation. Because of the above-mentioned historical bias, many of the studies on DNA methylation have been focused on CGIs at GPs and TSSs until quite recently, and this amount of work has shaped the general perceptions about the mechanisms and function of DNA methylation. Nevertheless, the advent of recent biotechnological tools that enable genome-wide studies of methylation patterns, such as bisulphite treatment (3), have allowed researchers to create a more realistic picture of the relationship between methylation and gene regulation. First, the methylation patterns of CpG dinucleotides that are situated in parts of the genome that are distinct from GPs and TSSs, including gene bodies, repeated regions such as centromeres, enhancers and insulators, are being assessed more frequently. Moreover, their effects on gene modulation and other important cell functions are becoming less established than what was initially predicted (4).

Another relevant aspect of methylation patterns concerns the link between aberrant methylation and disease (5). Perhaps the most relevant pathological outcome of aberrant methylation is cancer (5–7). In this regard, cancer cell promoters have been shown to be either hypo- or hypermethylated in CGIs (6). However, the observation that hundreds of epigenetically silenced genes may exist, even in individual tumours, has raised the question of whether they all cause tumourigenesis. Interestingly, tumour-cell precursors share many properties with healthy stem cells (6,7). Notably, one main difference in the epigenetic regulation of stem cells versus mature cells is the fact that in healthy

*To whom correspondence should be addressed. Tel: +39 02 6448 8025; Fax: +39 02 6448 8068; Email: luca.nardo@unimib.it

human stem and embryonic cells (8–11), methylation involves non-CpG dinucleotides. These methylation patterns, which are removed in mature differentiated tissues, appear to be at least partially conserved in cancer cells (7). This observation suggests that obtaining detailed knowledge of the topological distribution of methylation sites, particularly the relatively unexplored non-CpG methylation patterns, is a preliminary requirement for gaining a more exhaustive understanding of the molecular mechanisms underlying the critically important effects of physiological and pathological methylation. Namely, non-CpG methylation patterns should be mapped within specific genes over the entire genome with high statistical reliability and as a function of allelic variants, cell type, age and health status. Moreover, methylation changes can be potentially powerful prognostic and predictive markers for the diagnosis of neoplastic and imprinting diseases (12). For the above reasons, new labour- and cost-effective techniques permitting high-throughput determination of both single-locus and genome-wide methylation patterns are desired. Currently, the main methylome analysis techniques rely on bisulphite treatment of genomic DNA followed by PCR amplification (3,12–14). However, the necessity of changing the DNA sequence corresponding to the methylation sites prior to PCR makes it challenging to design primers and exposes the researcher to the risk of misinterpreting the data due to the so-called PCR bias, i.e. the tendency to preferentially amplify the sequence corresponding to one specific methylation pattern (12,15,16). Other currently applied techniques are the nearest-neighbour analysis technique (9,17) and the Luminometric Methylation Assay (LUMA) (10,11,18). Diede *et al.* (19) recently proposed that the differential stability of methylated versus non-methylated duplexes might be exploited to probe the amount of methylation in both specific genes and entire genomes in a smart and sensitive way. Indeed, substitution of methylcytosine for cytosine in the context of CpG repeats has been previously shown to enhance the double-strand stability during both thermal (20–22) and chemical denaturation (20,21,23). Notably, the results of Diede *et al.* may open the way to an entirely new class of methylation detection methods based on the evaluation of the stability of duplexes formed between the DNA under analysis and suitably designed oligonucleotide probes. Melting analysis should be feasible on non-amplified and/or non-purified DNA samples through the usage of the fluorescence resonance energy transfer (FRET) between fluorescent labels functionalizing the oligonucleotide probes and the application of advanced time-resolved fluorescence methods, analogous to the analysis that was previously demonstrated by members of our group (24).

The design of experimental protocols aimed at revealing the methylation state of natural DNA samples requires the optimal interaction of the oligonucleotide probes with the genomic template and the detailed knowledge about their annealing temperature. Therefore, a rational design of the probes devoted to the above-mentioned applications is not even conceivable without the ability to predict the melting temperature as a function of not only the template sequence but also its methylation patterns, as well as the position of the guanines within the probe that are destined to hybridize to the template methylcytosine residues. The currently available models for determining the annealing temperature of oligonucleotide probes are based on a semi-empirical determination of the entropy and enthalpy of hybridization for every possible dinucleotide pair (25–28). In the case of the reaction of the probe with a methylated template, these parameters should be corrected to account for the difference between the contributions of methylcytosine and cytosine. Notably, the development of models accounting for the contribution of methylation to the thermal stability of the probe-template duplexes could be used with the aim of overcoming the PCR bias in canonical methylation detection assays (29).

In the present work, we systematically analysed the thermal stability of the duplexes formed between an oligonucleotide probe dual labelled at its opposite ends with the donor and the acceptor of a FRET pair and complementary DNA oligomers containing non-CpG cytosine methylation patterns. Specifically, the donor fluorescence was measured and its properties analysed to extract the fraction of double-stranded-DNA (ds-DNA) probe as a function of temperature and the number of target-oligonucleotide methylations by both steady-state fluorimetry (SSF) and time-correlated single-photon counting (TCSPC). The most classical technique to assess the DNA melting temperature with high reproducibility and good temperature resolution uses the reduction in UV absorption at 260 nm (hypochromism) due to base-base stacking in the double-stranded DNA structure (19–22). Here we used this spectrophotometric method to validate our fluorimetric assay. With the aim of providing reliable estimations of the appropriate thermodynamic parameters for methylated TpC, CpT, ApC and CpA dinucleotides, we devised an original empirical model to account for the non-trivial phenomenology we observed. The model is able to predict the melting temperature of methylated oligonucleotides by assuming that the standard values of the hybridization entropy and enthalpy for dinucleotides containing a methylcytosine residue are increased by fixed factors. Such factors are determined by comparing our experimental melting temperature data with the homologous non-methylated data. We believe that in addition to confirming the ds-DNA-stabilizing action of methylcytosine also in the context of non-CpG sequences, the present investigation may provide new tools that foster research efforts devoted to elucidate the mechanisms of the fine regulation of gene expression exploiting intragenic methylation and the pathogenic potential of aberrant non-CpG methylation patterns. Specifically, the design of optimized site-specific probes and PCR primers for methylation pattern analyses may benefit from the ability of the proposed empirical model to predict methylation-corrected annealing temperatures.

MATERIALS AND METHODS

Oligonucleotides and sample preparation

Lyophilized samples of synthetic DNA were purchased from Sigma Genosys. The dual-labelled probe with the FRET donor and the acceptor bore no methylcytosine residues and was purified after fluorescent labelling by double Reverse Phase 1 (RP1) and HPLC procedures.

The donor was the commonly used fluorophore TAMRA, whereas the acceptor was the non-emitting polyaromatic azo compound Black-Hole Quencher 2 (BHQ2). The unlabelled complementary (target) oligonucleotides were desalted and methylated to various extents. We report the probe and targets sequences in Figure 1. The methylcytosine residues are indicated with an M. The supplier provided the buffer volume in which to resuspend each sample to obtain a 100 μM concentration. The resuspension buffer was 10 mM TE, pH 7.4. Annealing was performed by mixing equal volumes of the probe and target stock solutions (10 μl) and diluting the mixture with 16 μl of 150 mM phosphate-buffered saline, pH 7.4 and 4 μl of 10X TAQ buffer solution (Roche). The annealing ramp was executed with a Veriti thermocycler (Applied Biosystems). The samples were heated to 98°C to denature any residual intrastrand secondary structure, cooled at 1°C/min to the annealing temperature specified by the supplier for the non-methylated duplex (70°C), allowed to react at that temperature for 10 min and finally slowly cooled (1°C/min) to room temperature. The fluorescence measurements were performed on 50 nM concentrated samples, obtained by diluting the stocks in phosphate-buffered solutions at the desired ionic strength, prepared using suitable amounts of Na_2HPO_4 as the basic salt and KH_2PO_4 as the acidic salt (PBS). The pH of all the buffer was 7.6, whereas the total monocation concentration, I, ranged from 10 mM to 400 mM.

UV absorption and steady-state fluorimetry

UV-Vis absorption spectra were recorded with a Lambda 2 spectrophotometer (Perkin Elmer) equipped with a liquid-flow-thermostatable cell holder. Steady-state fluorescence spectra were acquired on a Cary Eclipse spectrofluorimeter (Varian) equipped with a 4-cell fluid-circulation temperature-controlled cell holder. Both the spectrophotometer and the fluorimeter cell holders were connected to a Julabo MA-F12 heater/chiller. The actual temperature of the sample was measured using a precision thermometer (Testo 735) equipped with a calibrated probe (Testo AG 310) that was placed in a hole in the cuvette holders. The temperature values measured each second by the AG 310 probe were read on the Testo 735 thermometer and sent to a PC, where they were registered by the Testo Comfort X35 software. The average value of the measured temperatures during each spectrum measurement was calculated and used as the nominal spectrum-acquisition temperature.

The samples were placed in hermetically sealed screw-top quartz cuvettes (Starna) to avoid artifacts due to buffer evaporation at high temperatures. The melting temperature of each duplex was derived by averaging the results of three independent denaturation experiments. The corresponding standard deviations were adopted as estimates of the experimental errors.

Time-correlated single photon counting measurements

Time-resolved fluorescence measurements were obtained by TCSPC, using a TCSPC setup that is fully described elsewhere (30–32) and has <30 ps temporal resolution (full-width at the half maximum of the temporal point-spread function). For the measurements presented in this paper, a mode-locked, frequency-doubled Nd:VAN laser (532 nm output wavelength) was used as the excitation source. The samples were held in a liquid-flow-thermostatable cell holder. The temperature was tuned with the same chiller and recorded with the same thermometer-software system as in the steady-state measurements.

TCSPC data analysis

The raw experimental TCSPC histograms were directly fitted to the following model function:

$$y(t) = A\sum_{i=1}^{N} f_i \exp\left(-\frac{t-t_0}{\tau_i}\right) + y_0 \qquad (1)$$

where the χ^2 value was minimized through a built-in Levenberg-Marquardt algorithm in MATLAB. In Equation (1), A is the total fluorescence pulse height at the excitation time, $t = t_0$. Consequently, f_i represents the desired fractional zero-time fluorescence amplitude (and, consequently, the relative concentration) of the different species, τ_i represents the decay time, and y_0 represents the constant background due to detector dark counts and non-time-correlated stray light. Also in this case, the melting temperature of each duplex was derived by averaging the results of three independent denaturation experiments. The corresponding standard deviations were adopted as estimates of the experimental errors.

RESULTS

Before applying our melting temperature detection assay to study the dependence of this thermodynamic parameter on the number and position of methylation sites, we deemed it necessary to rely on a subset of melting temperature values derived by a commonly applied technique, i.e. UV spectrophotometry, to which we refer to the aim of validating the fluorescence-based methods. In Figure 2 we report the melting curves derived by plotting the absorbance detected at 260 nm as a function of temperature in standard spectrophotometric thermal ramp experiments for target oligonucleotides (a), (b), (e) and (i) in Figure 1, hybridized to an unlabelled non-methylated complementary oligonucleotide. The solid lines represent best fitting curves to the following Boltzmann-like function, which is routinely used to model phase transitions and other sigmoidal trends (33–35):

$$A(260\ nm) = \varepsilon + \frac{\Delta}{1 + exp\left(-\frac{T-T_{den}}{\Delta T}\right)} \qquad (2a)$$

T_{den} is the melting temperature, and ΔT is the width of the transition. Here, ϵ represents the sigmoid asymptotic value at low temperatures, and $\epsilon+\Delta$ provides the asymptotic value at high temperatures. In analogy to early reports on natural CpG methylated DNA samples (20–22), we observe in Figure 2 a monotonic increase in T_{den} with the number of methyl-cytosines.

In Figure 3, we present the measured values of the steady-state fluorescence intensity at 580 nm of 50 nM solutions of free TAMRA, of the ss-DNA probe, and of the ds-DNA

PROBE:

TAMRA – 5′- GTG TGT GAG TGT GTG AGT GTG TGA GTG TGT GAG TGT GTG -3′- BHQ2

TARGET OLIGONUCLEOTIDES

(a)	Non-methylated:	CAC	ACA	CTC	ACA	CAC	TCA	CAC	ACT	CAC	ACA	CTC	ACA	CAC
(b)	1 methylation, central:	CAC	ACA	CTC	ACA	CAC	TCA	MAC	ACT	CAC	ACA	CTC	ACA	CAC
(c)	1 methylation, 5′:	MAC	ACA	CTC	ACA	CAC	TCA	CAC	ACT	CAC	ACA	CTC	ACA	CAC
(d)	1 methylation, 3′:	CAC	ACA	CTC	ACA	CAC	TCA	CAC	ACT	CAC	ACA	CTC	ACA	CAM
(e)	5 methylations, central:	CAC	ACA	CTC	ACA	CAC	TMA	MAM	AMT	MAC	ACA	CTC	ACA	CAC
(f)	5 methylations, 5′:	MAM	AMA	MTM	ACA	CAC	TCA	CAC	ACT	CAC	ACA	CTC	ACA	CAC
(g)	5 methylations, 3′:	CAC	ACA	CTC	ACA	CAC	TCA	CAC	ACT	CAC	ACA	MTM	AMA	MAM
(h)	5 methylations, distributed:	MAC	ACA	CTC	AMA	CAC	TCA	CAM	ACT	CAC	ACA	MTC	ACA	CAM
(i)	10 methylations, central:	CAC	ACA	CTC	AMA	MAM	TMA	MAM	AMT	MAM	AMA	CTC	ACA	CAC
(j)	10 methylations, lateral:	MAM	AMA	MTM	ACA	CAC	TCA	CAC	ACT	CAC	ACA	MTM	AMA	MAM
(k)	10 methylations, distributed:	MAC	AMA	CTM	ACA	MAC	TMA	CAM	ACT	MAC	AMA	CTM	ACA	MAC

Figure 1. Sequences of the dual-labelled probe and the differentially methylated target oligonucleotides. The methylcytosines are indicated with a red 'M'.

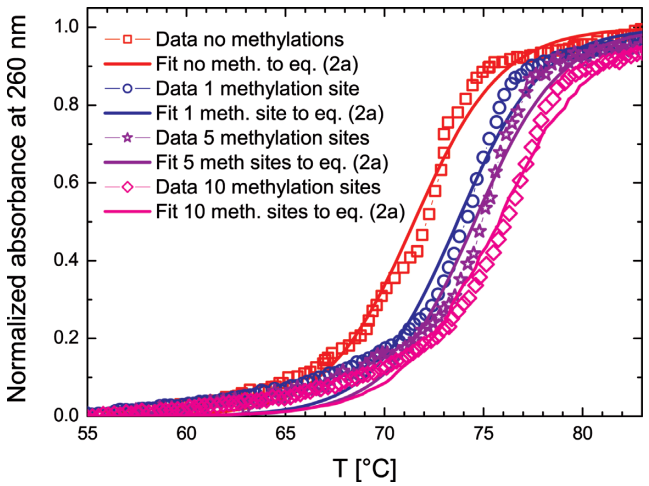

Figure 2. Denaturation data obtained from the measurement of UV absorbance at 260 nm versus temperature, T, for samples (a), (b), (e) and (i) (see Figure 1 for details). The solid lines represent the best fit of the experimental data to Equation (2a).

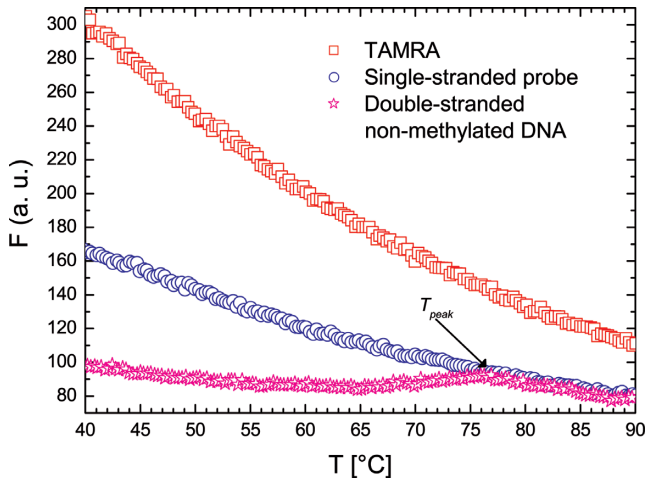

Figure 3. Steady-state fluorescence signal, F, measured as a function of temperature, T, for samples containing 50 nM concentrated free TAMRA (squares), TAMRA-labelled ss-DNA (circles) or TAMRA-labelled ds-DNA (stars, the probe was hybridized to target A), see Figure 1.

probe-target duplexes, as a function of temperature. The plotted data were obtained with bare (i.e. non-methylated target oligonucleotide) DNA in PBS at I = 150 mM. The first result shown in Figure 3 is that the fluorescence quantum yield of the widely used fluorescent label TAMRA is, by itself, strongly temperature dependent. The second observation is that at 40°C, i.e. only slightly above room temperature, in thermodynamic conditions in which optimal hybridization is expected for the duplex sample, the fluorescence of the ds-DNA sample is notably fainter than the fluorescence measured for the ss-DNA sample. The third result from the data in Figure 3 is that after a low temperature region where the ds-DNA and ss-DNA fluorescence values are clearly distinguishable and after a small peak (indicated by the arrow in Figure 3) in the ds-DNA fluorescence at approximately 75°C, the ss-DNA and ds-DNA fluorescence signals were superimposed at higher temperatures. This difference between the ds-DNA and ss-DNA data, which is only noticeable at low temperature, suggests that it is possible to quantitatively follow the denaturation reaction.

To confirm this assumption, we adopted a second data analysis procedure to characterize the melting phenomenon using our fluorescence data. This method considers the val-

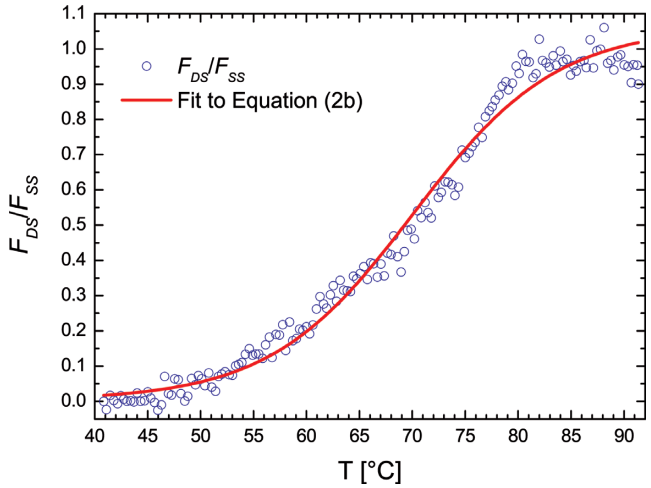

Figure 4. Sigmoidal denaturation plot obtained from the fluorescence versus temperature, T, data of Figure 3 by dividing the ds-DNA sample data, F_{DS}, by the corresponding single-stranded probe data, F_{SS}, as detailed in the text. The solid line represents the best fit of the experimental data to Equation (2b).

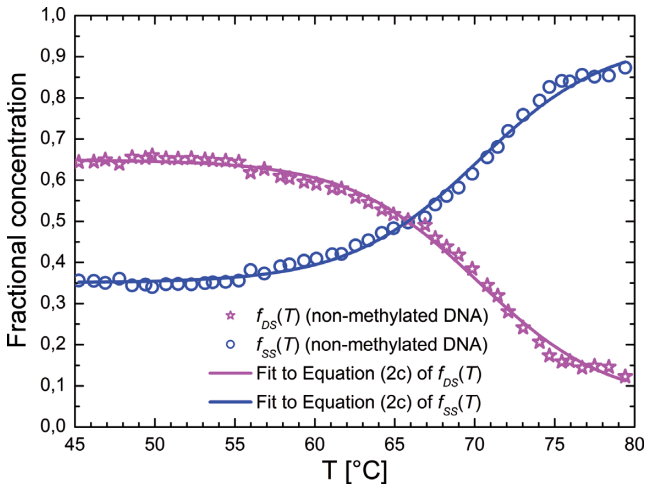

Figure 5. Fractional concentrations of ss-DNA, f_{SS} and ds-DNA, f_{DS}, obtained as a function of temperature, T, through the fitting of the time-resolved fluorescence decay data of a ds-DNA sample obtained by hybridization of the probe to target (a) of Figure 1, as detailed in the text. The solid lines represent the best fit of the experimental data to Equation (2c).

ues (F_{DS}/F_{SS}) obtained by point-by-point division of the duplex fluorescence signal (F_{DS}) by the ss-DNA probe signal (F_{SS}), which were further normalized to span a dynamic range from zero (maximally annealed sample, at low temperature) to one (fully denatured DNA, at high temperature). As shown in Figure 4, which was obtained by applying this normalization procedure to the data in Figure 3, the F_{DS}/F_{SS} plots display a sigmoid-like pattern that is readily interpreted in terms of a conformational transition, and the results are strongly reminiscent of the classical melting data typically obtained using UV absorption measurements (see Figure 2). Systematic deviations from symmetry with respect to the transition midpoint could make it difficult to precisely determine the transition temperature, but neglecting these deviations has made it possible to fit the Figure 4 data (and the homologous data obtained using other target samples) to the following equation, which represents a straightforward modification of Equation (2a).

$$\frac{F_{DS}}{F_{SS}} = \varepsilon + \frac{\Delta}{1 + exp\left(-\frac{T - T_{steady-state}}{\Delta T}\right)} \qquad (2b)$$

Here $T_{steady\text{-}state}$ is the temperature of transition midpoint as detected with our fluorimetric assay, and ΔT is the width of the transition. As in Equation (2a), ϵ represents the sigmoid asymptotic value at low temperatures, and $\epsilon+\Delta$ provides the asymptotic value at high temperatures. Although in both the present instances we fitted normalized data, we allowed the ϵ and Δ parameters to slightly vary during fitting. However, the fitting values were constrained within the interval $-0.05/+0.05$ and $0.95/1.05$, respectively, and the constraints were never reached.

The melting temperature values extracted by applying the above fitting procedure to the data obtained in different methylation conditions were compared with those obtained by determining the relative thermal stability of the same samples using the TCSPC technique. TCSPC requires a complex optical setup and very long acquisition times; these requirements are not compatible with parallel acquisition. However, TCSPC allows direct and simultaneous discrimination of the different fluorescent species present in a heterogeneous mixture. Indeed, the different fluorescent species reveal themselves as independent exponential components within the overall fluorescence decay pattern. Moreover, the fractional concentration of each species is directly derived from the experimental data using the relative amplitude of the corresponding exponential transient. In our case, the different species are the ds-DNA and ss-DNA oligomers, whose concentrations decrease and increase, respectively, as a function of temperature. Accordingly, the relative amplitude of the ds-DNA decay transient is expected to decrease sigmoidally with increasing temperature. In the Supplementary Materials, we discuss the TCSPC data at length, providing evidence that supports our attribution of each of the resolved decay components to a fluorescent species and describing the analysis procedures we applied to extract the denaturation curves from the rough decay patterns acquired at various temperatures. Here, we simply report the plot for a representative data set (i.e. bare DNA dissolved in PBS at I = 150 mM), and we proceed to compare the melting parameters pertaining to the TCSPC analysis with those provided by the other procedures. Namely, in Figure 5, we show the relative amplitudes of the decay components ascribed to the emission of TAMRA-labelled ds-DNA (magenta stars) and ss-DNA (blue dots) oligomers together with their best fits to the following equation:

$$f_i = \varepsilon_i + \frac{\Delta_i}{1 + exp\left(-\frac{T - T_{timing,i}}{\Delta T_i}\right)} \qquad (2c)$$

that represents a suitable modification of Equation (2). As expected, the relative amount of ds-DNA, f_{DS}, decreases as the temperature increases, whereas the opposite trend oc-

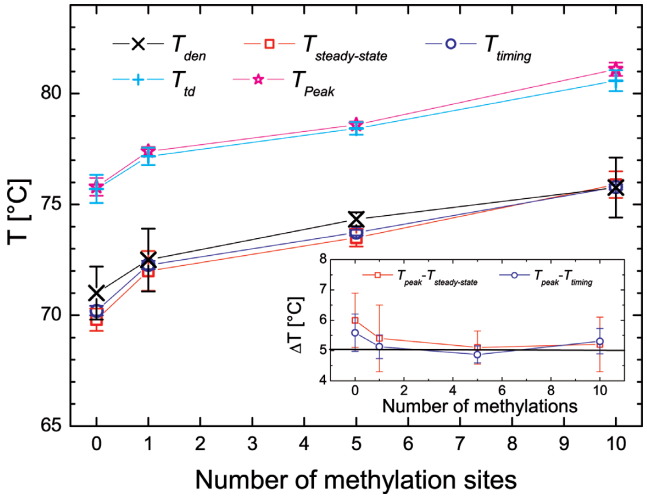

Figure 6. Comparison of the melting temperature values obtained for centrally methylated samples (a), (b), (e) and (i) of Figure 1 (0–10 methylations) in 150 mM PBS buffer with the different procedures detailed in the text. Crosses: melting temperatures, T_{den}, (black) and total denaturation temperatures, T_{td}, (cyan) obtained from the sigmoidal patterns obtained by processing the UV absorption data (Figure 2). Squares: melting temperatures, $T_{steady\text{-}state}$, obtained by fitting the sigmoidal patterns obtained by processing the steady-state fluorescence data (Figure 4). Circles: melting temperatures, T_{timing}, provided by fitting the denaturation plots obtained from the time-resolved measurements (see Figure 5). Stars: temperatures, T_{peak}, at which the steady-state fluorescence intensity patterns measured for the ds-DNA samples display a peak (Figure 3). Inset: differences between T_{peak} and $T_{steady\text{-}state}$ (squares) or T_{timing} (circles) at different methylation extents.

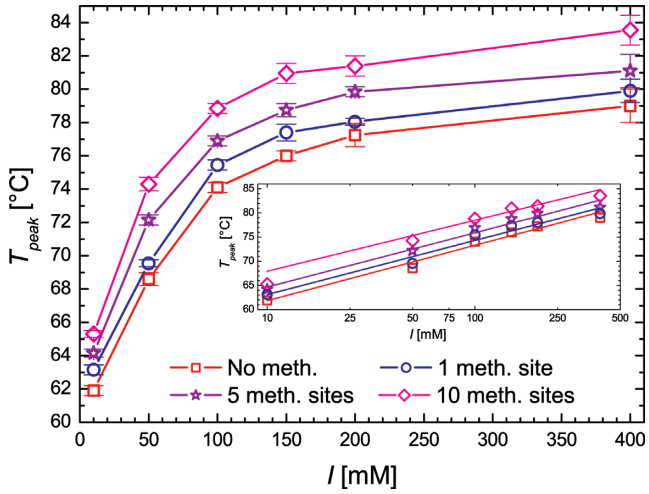

Figure 7. Values of T_{peak}, measured as a function of the ionic strength, I, for the duplexes formed by the dual-labelled probe with the non-methylated target oligonucleotide (a) of Figure 1 (squares), and with the target oligonucleotides (b), (e) and (i) of the same figure, containing one (circles), five (stars) and ten (diamonds) centrally located methylcytosine nucleotides, respectively. Inset: semi-logarithmic plot of the same data, together with their linear fits.

curs for the amount of ss-DNA, f_{SS}. Moreover, the obtained sigmoid-like plots are symmetric with respect to a common transition midpoint. A common fitting parameter, T_{timing}, is thus easily extractable using Equation (2c) as a fitting function. It should be noted that f_{SS} has a value of ≈0.35 even at room temperature. This indicates the presence of an aliquot of single-stranded probe near 35% in our samples even at temperatures close to body temperature, and might be the symptom of a non-optimized annealing protocol. On the other side, the sigmoidal trend typical of melting transitions is neatly reproduced and the significance of the derived melting temperature values is thus hardly questionable.

We can now compare the temperatures that have been obtained by the four procedures listed above and assumed as the melting indicators, namely T_{den} (see Figure 2), T_{peak} (see Figure 3 and the related discussion), $T_{steady\text{-}state}$ (Figure 4) and T_{timing} (Figure 5). This comparison is made explicit in Figure 6 for oligomers containing 0–10 centrally located methylation sites (see target sequences (a), (b), (e) and (i) in Figure 1), in PBS at I = 150 mM. We observe that all the $T_{steady\text{-}state}$ and T_{timing} values overlap within very limited experimental uncertainties. Moreover, they are very similar to the melting temperature values T_{den} derived for the corresponding duplexes from the spectrophotometric melting experiments. Moreover, although the T_{peak} values are systematically upshifted from a relatively constant value of approximately 5°C (see Figure 6 inset), the trend of T_{peak} versus the degree of methylation is identical to that exhibited by T_{den}, T_{timing} and $T_{steady\text{-}state}$. The upwards shift of T_{peak} with respect to both $T_{steady\text{-}state}$ and T_{timing}, which, coinciding with T_{den}, represent experimental assessments of the melting temperature, has a physical source. Indeed, T_{peak} can be identified as the temperature at which the melting transition is complete, as suggested by the similarity of the T_{peak} with the temperature values, T_{td}, at which the sigmoids obtained by spectrophotometric measurements reach their upper plateau (see Figure 6). The attribution to T_{peak} of the physical meaning of temperature of total denaturation will be further discussed in the Supplementary Materials section. Because we are interested in the relative shifts of the melting temperature at the various methylation levels and ionic strengths, the presence of a constant shift in the values of the melting temperature can be assumed not relevant. Thus, considering the superior simplicity of the experimental access of T_{peak}, which is readily obtained by merely localizing the fluorescence maximum within the SSF-versus-temperature raw data plots of the ds-DNA samples, we choose to adopt T_{peak} as the benchmark of the melting transition shifts.

Having defined and validated a procedure to obtain the melting temperature of the oligomers, we present in Figure 7 a systematic study of the thermal stability dependence on the ionic strength and methylation level. As shown in Figure 7, for all of the tested salt concentrations, the T_{peak} value monotonically increases with the number of methylation sites. Moreover, the methylation process does not seem to appreciably modify the dependence of the thermal stability on the salt concentration. Indeed, as shown in the semi-logarithmic plot of the inset in Figure 7, the theoretically predicted proportionality between the melting temperature and the logarithm of the ionic strength is preserved for the methylated oligonucleotides, and the slopes of the semi-logarithmic regression plots are relatively constant with the degree of methylation changes.

We now examine the dependence of the thermal stability on the position of the methylation sites along the DNA oligomer. In Figure 8A, B and C, the T_{peak} values at different ionic strengths are compared for the target oligonucleotides containing the same number of methylated cytosines (1 in Figure 8A, 5 in Figure 8B, and 10 in Figure 8C) either at a central position (blue squares), next to the oligonucleotide ends (red circles), or homogeneously distributed throughout the entire oligonucleotide (magenta stars, not pertinent to singly methylated samples). The thermal stability appears to be systematically enhanced when methylations occur next to either of the nucleotide ends. The effect of the even distribution of methylation sites throughout the oligonucleotide sequence is more controversial because it results in a significant increase in the thermal stability of the sample with 5 methylation sites; by contrast, for the samples with 10 methylation sites, the T_{peak} for the sample with evenly distributed methylation sites does not substantially differ from that of the centrally methylated sample.

DISCUSSION

There are several points that need to be addressed about the fluorescence data shown above. We first consider the temperature dependence of free TAMRA fluorescence shown in Figure 3. This behaviour was previously observed by other authors (36–39), and it is attributed either to the temperature-dependent pH of the buffer, leading to a differential dissociation equilibrium (37), or to internal conversion pathways involving an activation-potential inhibited excited-state intramolecular electron transfer from the amine group to the xanthene ring, whose rate is enhanced by increased temperature in agreement with the Arrhenius model (38,39). Alternatively, this effect may be ascribed to efficient S_1 deactivation through other internal conversion pathways, by which the electronic energy is initially transferred to highly excited vibrational modes of the ground electronic state and is eventually dissipated through collisional quenching by the solvent molecules, analogous to the process that was reported for other fluorescent xanthene dyes (40). The latter mechanism is obviously more efficient (and the fluorescence quantum yield is lower), such that the higher the probability of fluorophore-solvent collisions is, the higher the temperature. The temperature dependent fluorescence quantum yield exhibited by TAMRA is a drawback of this widely used fluorescent label, making the fluorophore possibly not the optimal probe for denaturation experiments. However, the temperature dependent fluorescence of TAMRA, although complicating the analysis, does not prevent to extract the desired information. Moreover, it should be mentioned that most of the commonly used DNA fluorescent labels, including several fluorescein and rhodamine derivatives, exhibit temperature dependent fluorescence. On the other side, our choice was driven by the consideration, on the basis of literature reports (41) confirmed ex-post by the data shown in Figure 6, that labelling with TAMRA assures minimal perturbation of the duplex stability. Furthermore, TAMRA combines desirable time-resolved fluorescence properties (namely single exponential decay with a lifetime significantly shorter than the pulse period of common solid state picosecond pulsed lasers used for TCSPC, which assures optimal decay analysis and minimal fluorescence pile-up effects) with a high quantum yield (0.8) and an excitation wavelength at which the absorption of endogenous fluorophores is negligible. Also the above characteristics made us propend for the choice of TAMRA as the fluorescence reporter, in view of possible future diagnostic applications to the detection of the degree of methylation of medically relevant DNA traits (e.g. oncogene promoters) on non-purified and non-amplified genomic templates, in analogy to the method proposed in (24) for molecular typing of polymorphic genes.

The second interesting phenomenon shown in Figure 3 is the unexpected reduction of the ds-DNA fluorescence signal with respect to the ss-DNA signal at low temperature. This decrease occurs despite the larger persistence length of the ds-DNA (≈50 nm, corresponding to 150 bp) compared with the ss-DNA (≈2.5 nm, corresponding to only 4 bp, according to (42)), which implies that the distance between TAMRA and BHQ2 is larger (and the FRET quenching is less effective) in the double-stranded structure (see Supplementary Material for details). Thus, it seems that the most important factor in the TAMRA quenching is not the distance between the TAMRA and BHQ2 molecules but the presence of the ds-DNA near the TAMRA molecule. In the Supplementary Materials (see Paragraph 5) we present fluorescence-versus-temperature plots similar to the ones of Figure 3 obtained for the non-methylated target oligonucleotide hybridized to a probe singly-labelled at its 5′ end with TAMRA (i.e. lacking the BHQ2 in 3′). These data exhibit reduced fluorescence for the ds-DNA specimen with respect to the ss-DNA sample and a peak in the fluorescence versus temperature plot for the ds-DNA located at the same T_{peak} as the corresponding dual-labelled oligonucleotide. In the Supplementary Materials, we also show fluorescence decays at room temperature for the same samples. Overall these data demonstrate that FRET of TAMRA fluorescence by BHQ2 is actually negligible in the ds-DNA configuration. Behaviour very similar to this, i.e. a consistent reduction in TAMRA fluorescence upon ds-DNA formation, was very recently reported for a DNA-melting experiment with TAMRA-labelled oligonucleotides (43). In this paper, the typical tendency of TAMRA to be oxidized by guanine bases through excited-state photo-electron transfer (PET) and the reported reduced fluorescence quantum yield of the oxidized TAMRA state (44,45) were claimed to be the molecular mechanisms underlying this unconventional phenomenology. The probability of this photochemical reaction is enhanced in a geometry in which the dye and guanine molecular dipole moments are coplanar, i.e. in the double-stranded structure. In this type of structure, TAMRA is rotationally coupled to the oligonucleotide and is proposed to be stacked to the bases when it labels the 5′ end of guanine-rich oligonucleotides (46). It may be argued that in such a picture in which TAMRA fluorescence is quenched in the ds-DNA configuration more efficiently than in the ss-DNA configuration, and by mechanisms which do not depend from the presence of a FRET acceptor, further labelling of the oligonucleotide probe with BHQ2 is detrimental, as it lowers the signal-to-noise ratio in SSF measurements of the melting transition. However, we chose to work with dual-labelled probes because we had previous experience of the

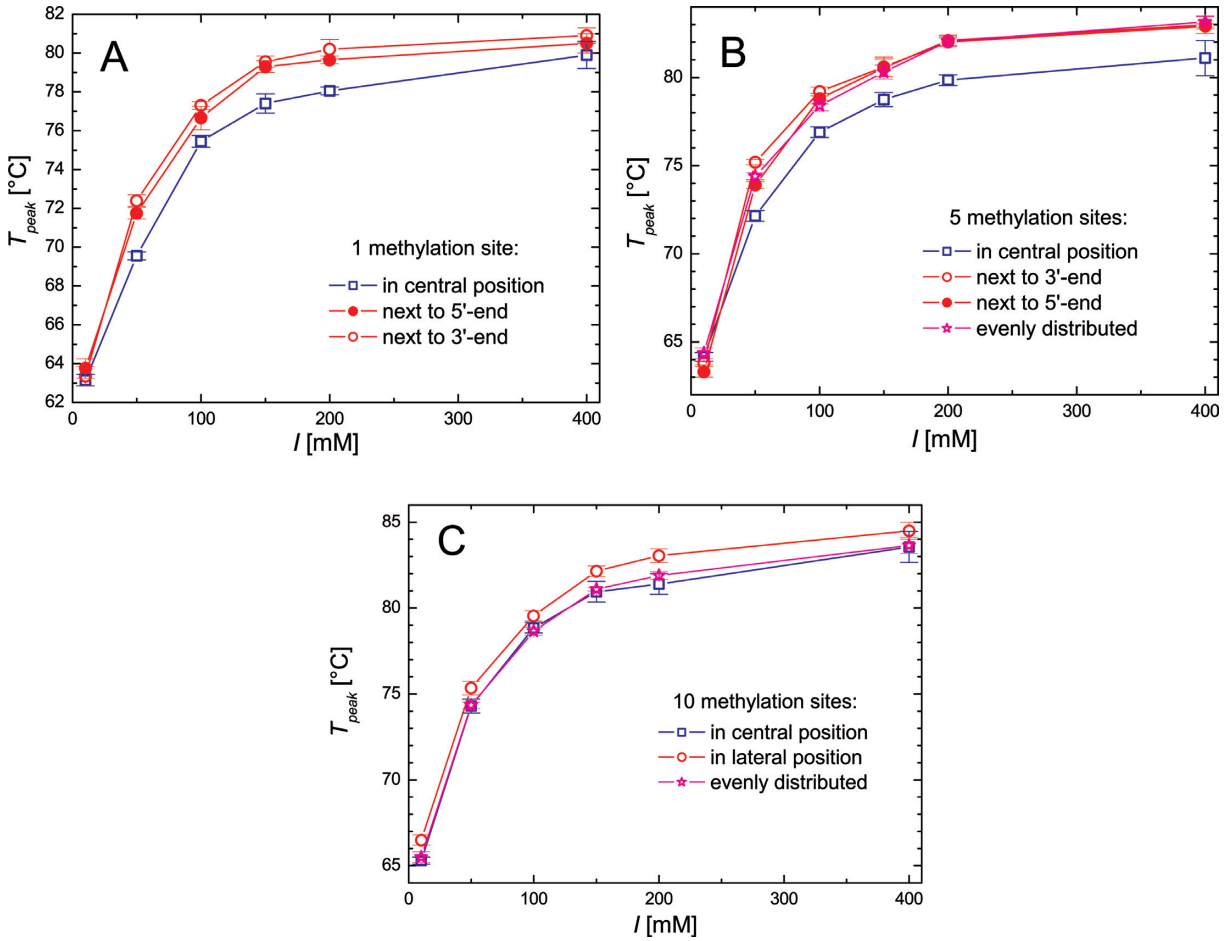

Figure 8. Dependence of T_{peak} on the position of methylation sites for oligonucleotides with a fixed number of methylation sites. The denaturation experiments were performed at different ionic strength, *I*, values using duplexes that contained the same number of methylcytosines, namely, 1 (panel (**A**), target oligonucleotides (b), (c) and (d) in Figure 1), 5 (panel (**B**), target oligonucleotides (e), (f), (g) and (h)) and 10 (panel (**C**), target oligonucleotides (i), (j) and (k)), either in the central position (squares), next to the oligonucleotide ends (dots and circles for the 3′ and 5′ ends, respectively), or evenly distributed throughout the oligonucleotide (stars). For 10 methylation sites, the effects of methylation in the lateral position were only evaluated for one oligonucleotide, with 5 methylcytosines at each end (see Figure 1 for details).

presence of residual free dye in substantial amounts in similar samples provided by both the same and other suppliers (24,30,31). Indeed, as detailed in Supplementary Materials, also in the present experiments we detect a relative concentration of roughly 20% free TAMRA by both TCSPC and an independent fluorescence analysis technique, fluorescence correlation spectroscopy. Only the presence of the BHQ2 allowed us to discriminate the fraction of TAMRA attached to ss-DNA from that of residual free TAMRA in the whole temperature range by TCSPC experiments.

Concerning the various suggested methods for extracting the DNA melting temperature, the proposed process for normalizing the steady-state fluorescence data shown in Figure 3 was already introduced by Liu *et al.* (36). They proposed a protocol for minimizing the bias in evaluating the transition temperature from melting curves obtained with gel-based DNA microchips by using fluorescent labels with temperature-dependent emission. Their protocol essentially consists of dividing the point-by-point fluorescence signal from the duplex sample by the signal from the free label at the same temperature. Our only modification was to substitute the free label signal with that of the dual-labelled single-stranded oligonucleotide, in order to account for the BHQ2 effects on the TAMRA fluorescence. As reported above in the comment to Figure 4, our normalized F_{DS}/F_{SS} data do not perfectly follow a sigmoidal trend, which is typical of classical phase transitions; instead, there are some deviations at low temperature. The perturbations can be attributed to the superposition of an additional, peculiar fluorescence quenching mechanism (namely PET) in the double-stranded conformation, which invalidates the previously proposed sigmoid-retrieval procedure (36). Indeed, this procedure is based on the implicit assumption that the temperature dependence of the fluorescence signal is inherently due to the fluorophore and is thus independent of conformation. In particular, we find that the asymmetries are more pronounced for samples with higher degrees of methylation and for buffers with higher ionic strength. This observation suggests that the PET reactions are maximally efficient in these circumstances (see Supplementary Material for details).

Nonetheless, the possibility of using a technique such as steady-state spectrofluorimetry would facilitate the experimental task of obtaining a systematic and statistically reliable analysis of the role of methylation in the thermodynamic stability of the double-helical structure. This technique is faster and easier to implement with respect to TCSPC, allows to work with lower amounts of DNA with respect to UV spectrophotometry and, at difference with both TCSPC and UV absorption, may be adapted to straightforward multiplexing. For this reason, we decided to use the raw fluorescence versus temperature data collected for the ds-DNA samples and to use the temperature corresponding to the ds-DNA maximum fluorescence intensity (T_{peak}) as a benchmark of the ds-DNA to ss-DNA phase transition. The T_{peak} parameter can be evaluated more precisely with respect to the midpoints $T_{steady\text{-}state}$ of the reconstructed sigmoids (see Supplementary Material for details). Furthermore, the physical interpretation of T_{peak} and its correlation with the melting process has been investigated by comparisons with the TCSPC data. This investigation resulted in the identification of T_{peak} with the temperature at which the melting transition is completed. Indeed, T_{peak} coincides with the temperature at which the TCSPC sigmoids reach the denaturation plateau for all of the samples that were subjected to both the SSF and TCSPC analyses, namely those consisting of oligonucleotides containing 0–10 methylated cytosines at the central position, at 150 mM ionic strength (see Supplementary Material for details).

From the biological standpoint, the confirmation of a stabilizing effect of the ds-DNA structure by cytosine methylation also in the context of non-CpG dinucleotides suggests that this physical modification plays a role in determining the peculiar characters of the epigenetics of stem cells and cancer-cell precursors. We remind that exclusively the latter two classes of cells exhibit widespread non-CpG methylation patterns within gene bodies, while they lack some of the fundamental methylation patterns displayed by mature healthy cells in CpG islands, and associated to both gene silencing and differentiation. The question arises whether non-CpG methylation partially fulfils the regulatory functions of CpG island methylation while assuring a higher degree of flexibility and reversibility. Indeed, while CpG methylation of gene promoters mainly results in permanent gene silencing, the currently available pioneering evidences on non-CpG intragenic methylation provide a wider panorama of their biological effects, and suggest a role of fine-tuning of the transcription kinetics for these epigenetic hallmarks. Moreover, non-CpG methylation is reversible and demethylases have been isolated devoted to removal of non-CpG methylation patterns. Because non-CpG methylation occurs mainly within gene bodies, it should be able to interfere with the activity of proteins devoted to transcription when they are already complexed with DNA, thus by exploiting different mechanisms with respect to the bare protein binding inhibition effect being the basic feature of CpG methylation at promoters. We can only speculate that a different thermodynamic stability of the ds-DNA structure might determine the inability for proteins performing a pivotal role in transcription, such as RNA polymerases and helicases, of locally separating the DNA strands, which in turn is propaedeutic to ribonucleotides pairing and mRNA synthesis. Indeed, it has been demonstrated that the processivity of helicases is strongly affected by increases of the force needed for strand separation in its substrate DNA of only a few piconewtons (47,48). Similar considerations might be extended to DNA replication, given that both DNA helicases and DNA polymerases are similarly sensitive to ds-DNA stability. For these more characterized systems it has even been shown that there exists a threshold force that the protein can act onto the DNA substrate in order to induce local strand separation. Beyond such threshold the protein simply results to be inactive. Namely, for T7 DNA polymerase the threshold force was quantified in 34 ± 8 pN by optical tweezers measurements (49).

Finally, it should be noted that the increment in thermal stability upon methylation might be due to either variations in the enthalpic term, in the entropic term or both in the Gibbs free energy variation. Modifications in the differential entropy between ds-DNA and ss-DNA might correspond to a variation in either the stiffness of the ds-DNA, that of the ss-DNA, or both. These alterations in the local mechanical and structural properties of DNA might interfere with the functionality of proteins whose structure is optimized to act on B-stranded DNA. Thus, in this picture thermal stabilization might be at least partially a 'side effect' of the actual mechanism of regulation tuning subtended to intragenic methylation rather than the mechanism itself, being the latter nano-mechanical rather than thermodynamic in nature. Indeed, literature data (50) evidenced that methylated ds-DNA has a substantially higher persistence length than non-methylated DNA.

An interesting finding of the data is the dependence of T_{peak} on the position of the methylated sites (see Figure 8A, B and C). Actually, this observation agrees with previous results obtained by Severin *et al.* (51), who applied force-spectroscopy methods to methylated DNA oligomers. Namely, they denatured oligonucleotide duplexes of 20 bases methylated in either central or lateral position by inducing shear stresses using a molecular force assay technique devised by their group (52). Briefly, in their experiments the differential stability of methylated versus non-methylated oligonucleotides was probed by using a central DNA single-stranded filament that began and ended with two equal 20 base sequences and had a central spacer of 13 thymine bases. Thymine 7 of the central spacer was labelled with the fluorophore Cy5. The lateral initial and terminal sequences were hybridized to the methylated and the non-methylated oligonucleotide under study, respectively. Each of the oligonucleotides under study was linked to a separate multiwell plate through a single-stranded spacer of 10 thymine bases at one end, and labelled at the other end with a Cy3 fluorophore, so that upon hybridization with the central spacer Cy5 acted as a FRET quencher for both the Cy3. The central filament was not attached to any of the plates. The plates could be moved far apart from one another by means of a piezoelectric device. The fluorescence intensity detected on the two plates after inducing the stress was inversely proportional to the number of central filaments that remained attached to that plate. Thus, the ratio between the fluorescence measured on the plate functionalized with the non-methylated oligonucleotide and that measured on the plate functionalized with the methylated oligonu-

cleotide was indicative of the relative stability of the methylated compared to the non-methylated duplex. Although these force spectroscopy results are hardly comparable with our melting temperature data, and even considering that the direction of application of the nanomechanical stress (e.g. shearing or unzipping) considerably affects the denaturation energetics, the authors observed a ≈40% increase in the fraction of filaments remaining attached to the methylated sequence by moving the methylation site from the centre to the ends of the probe oligonucleotide.

From a physical standpoint, the increase in T_{peak} observed when the methylated bases are in lateral position rather than in central position may be a consequence of the fact that denaturation likely begins next-to the duplex ends and propagates towards the oligonucleotide centre. Thus, reinforcing the bonds at lateral position has greater overall stabilizing effect. It should be noted that this border effect, which is notable as far as oligonucleotides are considered, is unlikely to play a major role in most biological systems, where DNA filaments are typically very long. Moreover, in living cells DNA assumes the single-stranded configuration only locally in melting bubbles, thus the opposite mechanism (i.e. denaturation starting from the centre rather than from the ends of a filament) takes place. Nevertheless, such phenomenon might have a relevance in a few important metabolic processes in which short DNA or RNA fragments interact with genomic DNA. However, we believe that taking this phenomenon into account is crucial, e.g. in designing oligonucleotide probes targeting differentially methylated genomic traits for diagnostic purposes, or PCR primers devoted to the targeting of methylated templates.

In the search for a rationale for this highly complex phenomenology, we developed a simple heuristic model that describes the effects of methylation on melting temperature in terms of the variations in the enthalpy and free energy of hybridization of the methylcytosines with respect to cytosine. Generally, according to classical theoretical models, the melting temperature of non-methylated DNA oligomers can be easily evaluated by considering the values of the enthalpy changes, ΔH°, and the free energy changes, ΔG°, for two different contributions at the temperature T° of the reference state: the contribution of base-pair initiation and the contribution of the 10 standard nearest-neighbour pairs (AA, AT, TA, CA, GT, CT, GA, CG, GC and GG) (25–28). Note that the additional contribution of the dangling end interactions quoted in these references is not pertinent to our case because the template DNA consists of an oligonucleotide with exactly the same length as the probe (35,53). Based on the enthalpy and melting data, there are several tables of nearest-neighbour interactions that allow us to calculate the DNA melting temperature given the base sequence of the oligomer. Some of the most widely used tables were revised in a previous study (28). To quantitatively evaluate the influence of methylation on the oligomer melting temperature, we assumed that cytosine methylation influences the ΔH° and ΔG° values of the involved methylated pairs (see Supplementary Material for details). Actually, in our specific oligomer, there are only four methylated pairs: MA, AM, MT, TM, where M is methylated cytosine. The MG, GM and MM pairs are not present. We used the ΔH° and ΔG° set of Quartin and Wetmur (26) and assumed

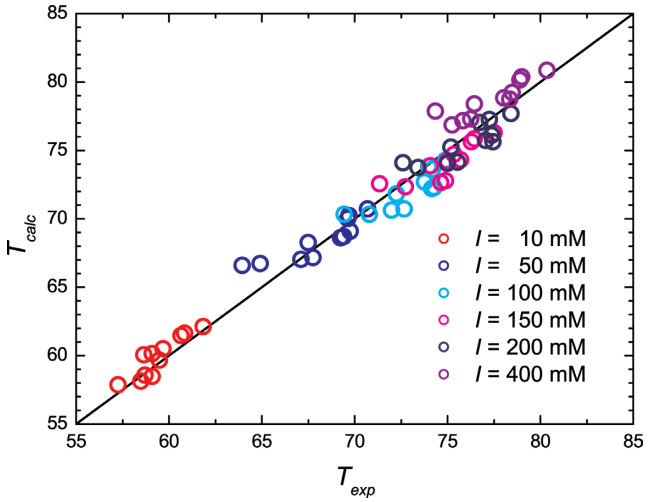

Figure 9. Methylated DNA melting temperature predictions compared to the experimental results. The predicted melting temperature, T_{calc}, is plotted versus the experimentally measured melting temperature, $T_{exp} = T_{peak} - 5°C$, at six ionic strengths represented by various colours. The continuous line represents the x = y line to emphasize the correspondence between the predicted and measured values.

an increase of a constant factor α for ΔH° and of a constant factor β for ΔG° for any methylated pair with respect to the corresponding non-methylated pair. Further imposing an increase of two 'edge stabilization' constants, δ and ϵ for ΔH° and ΔG°, respectively, in the case of oligomers beginning or ending with a methylcytosine residue, respectively, we obtained a reasonable agreement between the theory and the experiments. Namely, assuming the fitting values $\alpha = 1.4$, $\beta = 1.4$, $\delta = 0.4$ kcal/mol and $\epsilon = 0.4$ kcal/mol, we obtained the plot shown in Figure 9, where the calculated melting temperature, T_{calc}, is plotted as a function of the measured melting temperature $T_{exp} = T_{peak} - 5°C$. The continuous line in Figure 9 is the x = y line that equally divides the first quadrant. The superposition of the (T_{exp}; T_{calc}) points to such line with the exception of some non-systematic deviations supports the accuracy of the model in replicating the experimental results. It should be noted that the parameters we have derived provide a picture in which the main contribution to the thermodynamic stabilization observed upon methylation is enthalpic, while the entropic term plays against thermal stabilization upon methylation (ΔS is more positive for methylated pairs than for the corresponding non-methylated pairs). This result is in agreement with the previously reported increase in stiffness of methylated ds-DNA (50).

CONCLUSION

In this work, we systematically studied the thermal stability of a 39-bp oligonucleotide duplex as a function of the density and position of methylcytosine residues occurring within non-CpG pairs. The temperatures for complete duplex melting were determined by monitoring the variations in the fluorescence of a chromophore covalently linked to the 5′ end of one of the strands in the presence of a fluorescence quencher labelling the opposite end of

the same strand. Methylation progressively stabilized the double-helical structure, without interfering with the dependence of the melting on buffer salt concentration. Moreover, an incremental stabilization was observed for methylations occurring next to the oligonucleotide ends with respect to methylations at central positions. An empirical model was implemented to account for the effects of methylation on the melting temperature in terms of the variations in the entropy and enthalpy of hybridization of methylcytosine. The reported results confirm the ds-DNA stabilizing action of methylcytosine, and, in the future, may shed new light on the mechanisms for the fine regulation of gene expression that are connected to the non-CpG intragenic methylation of stem cell and cancer cell precursor genomes. Moreover, the results may help in designing site-specific probes for the assessment of both physiological and aberrant non-CpG methylation patterns through denaturation-ramp-based methods.

SUPPLEMENTARY DATA

Supplementary Data are available at NAR Online.

ACKNOWLEDGEMENT

We thank M. G. Cerrito and R. Giovannoni for useful discussions and suggestions, M. Longhi for help with the measurements.

FUNDING

Funding for open access charge: University of Milano Bicocca.
Conflict of interest statement. None declared.

REFERENCES

1. Holliday,R. and Pugh,J.E. (1975) DNA modification mechanisms and gene activity during development. *Science*, **187**, 226–232.
2. Riggs,A.D. (1975) X inactivation, differentiation, and DNA methylation. *Cytogenet. Cell Genet.*, **14**, 9–25.
3. Deng,J., Shoemaker,R., Xie,B., Gore,A., LeProust,E.M., Antosiewicz-Bourget,J., Egli,D., Maherali,N., Park,I.-Y., Yu,J. *et al.* (2009) Targeted bisulfite sequencing reveals changes in DNA methylation associated with nuclear reprogramming. *Nat. Biotech.*, **27**, 353–360.
4. Suzuki,M.M. and Bird,A. (2008) DNA methylation landscapes: provocative insights from epigenomics. *Nat. Rev. Genet.*, **9**, 465–476.
5. Robertson,K.D. (2005) DNA methylation and human disease. *Nat. Rev. Genet.*, **6**, 597–610.
6. Ohm,J.E., McGarvey,K.M., Yu,X., Cheng,L., Schuebel,K.E., Cope,L., Mohammad,H.P., Chen,W., Daniel,V.C., Yu,W. *et al.* (2007) A stem cell-like chromatin pattern may predispose tumor suppressor genes to DNA hypermethylation and heritable silencing. *Nat. Genet.*, **39**, 237–242.
7. Jones,P.A. and Baylin,S.B. (2007) The epigenomics of cancer. *Cell*, **128**, 683–692.
8. Lister,R, Pelizzola,M., Dowen,R.H., Hawkins,R.D., Hon,G., Tonti-Filippini,J., Nery,J.R., Lee,L., Ye,Z., Ngo,Q.-M. *et al.* (2009) Human DNA methylomes at base resolution shows widespread epigenomic differences. *Nature*, **462**, 315–322.
9. Ramsahoye,B.H., Biniszkiewicz,D., Lyko,F., Clark,V., Bird,A.P. and Jaenisch,R. (2000) Non-CpG methylation is prevalent in embryonic stem cells and may be mediated by DNA methyltransferase 3a. *Proc. Natl. Acad. Sci. U.S.A.*, **10**, 5237–5242.
10. Yan,J., Zierath,J. and Barrès,R. (2011) Evidence for non-CpG methylation in mammals. *Exp. Cell Res.*, **317**, 2555–2561.
11. Barrè,R., Osler,M.E., Yan,J., Rune,A., Fritz,T., Caidahl,K., Krook,A. and Zierath,J.R. (2009) Non-CpG methylation of the PGC-1α promoter through DNMT3B controls mitochondrial density. *Cell Metab.*, **10**, 189–198.
12. Wojdacz,T.K., Dobrovic,A. and Hansen,L.L. (2008) Methylation-sensitive high-resolution melting. *Nat. Prot.*, **3**, 1903–1908.
13. Wojdacz,T.K. and Hansen,L.L. (2006) Techniques used in studies of age-related DNA methylation changes. *Ann. N.Y. Acad. Sci.*, **1067**, 479–487.
14. Herman,J.G., Graff,J.R., Myohanen,S., Nelkin,B.D. and Baylin,S.B. (1996) Methylation specific PCR: a novel PCR assay for methylation status of CpG islands. *Proc. Natl. Acad. Sci. U.S.A.*, **93**, 9821–9826.
15. Warnecke,P.M., Stirzaker,C, Melki,J.R, Millar,D.S., Paul,C.L. and Clark,S.J. (1997) Detection and measurement of PCR bias in quantitative methylation analysis of bisulphite-treated DNA. *Nucleic Acids Res.*, **25**, 4422–4426.
16. Warnecke,P.M., Stirzaker,C., Song,J., Grunau,C., Melki,J.R. and Clark,S.J. (2002) Identification and resolution of artifacts in bisulfite sequencing. *Methods*, **27**, 101–107.
17. Gruenbaum,Y., Stein,R., Cedar,H. and Razin,A. (1981) Methylation of CpG sequences in eucariotic DNA. *FEBS Lett.*, **124**, 67–71.
18. Karimi,M., Johansson,S., Stach,D., Corcoran,M., Grander,D., Shalling,M., Bakalkin,G., Lyko,F., Larsson,C. and Ekstrom,T.J. (2006) LUMA (LUminometric Methylation Assay) – a high throughput method to the analysis of genomic DNA methylation. *Exp. Cell Res.*, **312**, 1989–1995.
19. Diede,S.J., Guenthoer,J., Geng,L.N., Mahoney,S.E., Marotta,M., Olson,J.M., Tanaka,H. and Tapscott,S.J. (2010) DNA methylation of developmental genes in pediatric medulloblastomas identified by denaturation analysis of methylation differences. *Proc. Natl. Acad. Sci. U.S.A.*, **107**, 234–239.
20. Ehrlich,M., Ehrlich,K. and Mayo,J.A. (1975) Unusual properties of the DNA from Xanthomonas phage XP-12 in which 5-methylcytosine completely replaces cytosine. *Biochim. Biophys. Acta*, **395**, 109–119.
21. Gill,J.E., Mazrimas,J.A. and Bishop,C.C. Jr (1974) Physical studies on synthetic DNAs containing 5-methylcytosine. *Biochim. Biophys. Acta*, **335**, 330–348.
22. Szer,W. and Shugar,D. (1966) The structure of poly-5-methylcytidylic acid and its twin-stranded complex with poly-inosinic acid. *J. Mol. Biol.*, **17**, 174–187.
23. Laprise,S.L. and Gray,M.R. (2007) Covalent genomic DNA modification patterns revealed by denaturing gradient gel blots. *Gene*, **391**, 45–52.
24. Nardo,L., Tosi,G., Bondani,M., Accolla,R. and Andreoni,A. (2012) Typing of a polymorphic human gene conferring susceptibility to insulin-dependent diabetes mellitus by picosecond-resolved FRET on non-amplified genomic DNA. *DNA Res.*, **19**, 347–355.
25. Breslauer,K.J., Frank,R., Blocker,H. and Marky,L.A. (1986) Predicting DNA duplex stability from the base sequence. *Proc. Natl. Acad. Sci. U.S.A.*, **83**, 3746–3750.
26. Quartin,R.S. and Wetmur,J.G. (1989) Effect of ionic strength on the hybridization of oligodeoxynucleotides with reduced charge due to methylphosphonate linkages to unmodified oligodeoxynucleotides containing the complementary sequence. *Biochemistry*, **28**, 1040–1047.
27. Blake,R.D. and Delcourt,S.G. (1998) Thermal stability of DNA. *Nucleic Acids Res.*, **26**, 3323–3332.
28. SantaLucia,J. Jr (1998) A unified view of polymer, dumbbell, and oligonucleotide DNA nearest-neighbor thermodynamics. *Proc. Natl. Acad. Sci. U.S.A.*, **95**, 1460–1465.
29. Shen,L., Guo,Y., Chen,X., Ahmed,S. and Issa,J.P. (2007) Optimizing annealing temperature overcomes bias in bisulfite PCR methylation analysis. *Biotechniques*, **42**, 48–52.
30. Andreoni,A., Bondani,M. and Nardo,L. (2009) Feasibility of single-probe SNP genotyping by time-resolved FRET. *Mol. Cell. Probes*, **23**, 119–121.
31. Andreoni,A., Bondani,M. and Nardo,L. (2009) A time-resolved FRET method for HLA DQB1 allele molecular typing by a single oligonucleotide probe. *Photochem. Photobiol. Sci.*, **8**, 1202–1206.
32. Maspero,A., Giovenzana,G., Masciocchi,N., Palmisano,G., Comotti,A., Sozzani,P., Bassanetti,I. and Nardo,L. (2013) Möhlau's anthradipyrazole revisited: a new look at an old molecular system. *Cryst. Growth Des.*, **13**, 4948–4956.

33. Tichopad,A., Dilger,M., Schwarz,G. and Pfaffl,M.W. (2003) Standardized determination of real-time PCR efficiency from a single reaction set-up. *Nucleic Acids Res.*, **31**, e122.
34. Navarro-Verdugo,A.L., Goycoolea,F.M., Romero-Meléndez,G., Higuera-Ciapara,I. and Arguelles-Monal,W. (2011) A modified Boltzmann sigmoidal model for the phase transition of smart gels. *Soft. Matt.*, **7**, 5847–5853.
35. Di Michele,L., Mognetti,B.M., Yanagishima,T., Varilly,P., Ruff,Z., Frenkel,D. and Eiser,E. (2014) Effects of inert tails on the thermodynamics of DNA hybridization. *J. Am. Chem. Soc.*, **136**, 6538–6541.
36. Liu,W.-T., Wu,J.-H., Sze-Ying,E. and Selamat,E.S. (2005) Emission characteristics of fluorescent labels with respect to temperature changes and subsequent effects on DNA microchip studies. *Appl. Environ. Microbiol.*, **71**, 6453–6457.
37. Duhr,S., Arduini,S. and Braun,D. (2004) Thermophoresis of DNA determined by microfluidic fluorescence. *Eur. Phys. J. E.*, **15**, 277–286.
38. Vamosi,G., Gohlke,C. and Clegg,R.M. (1996) Fluorescence characteristics of 5-carboxytetramethylrhodamine linked covalently to the 5′ end of oligonucleotides: multiple conformers of single-stranded and double-stranded dye-DNA complexes. *Biophys. J.*, **71**, 972–994.
39. Unruh,J.R., Gokulrangan,G., Wilson,G.S. and Johnson,C.K. (2005) Fluorescence properties of Fluorescein, Tetramethylrhodamine and Texas Red linked to a DNA aptamer. *Photochem. Photobiol.*, **81**, 682–690.
40. Martin,M.M. (1975) Hydrogen bond effects on radiationless electronic transitions in xanthene dyes. *Chem. Phys. Lett.*, **35**, 105–111.
41. Moreira,B.G., You,Y., Behlke,M.A. and Owczarzy,R. (2004) Effects of fluorescent dyes, quenchers, and dangling ends on DNA duplex stability. *Biochem. Biophys. Res. Comm.*, **327**, 473–484.
42. Murphy,M.C., Rasnik,I., Cheng,W., Lohman,T.M. and Ha,T. (2004) Probing single-stranded DNA conformational flexibility using fluorescence spectroscopy. *Biophys. J.*, **86**, 2530–2537.
43. Yin,Y., Yang,L., Zheng,G., Gu,C., Yi,C., He,C., Gao,Y.Q. and Zhao,X.S. (2014) Dynamics of spontaneous flipping of a mismatched base in DNA duplex. *Proc. Natl. Acad. Sci. U.S.A.*, **111**, 8043–8048.
44. Edman,L., Mets,U. and Rigler,R. (1996) Conformational transitions monitored for single molecules in solution. *Proc. Natl. Acad. Sci. U.S.A.*, **93**, 6710–6715.
45. Torimura,M., Kurata,S., Yamada,K., Yokomaku,T., Kamataga,Y., Kanagawa,T. and Kurane,R. (2001) Fluorescence-quenching phenomenon by photoinduced electron transfer between a fluorescent dye and a nucleotide base. *Anal. Sci.*, **17**, 155–160.
46. Unruh,J.R., Gokulrangan,G., Lushington,G.H., Johnson,C.K. and Wilson,G.S. (2005) Orientational dynamics and dye-DNA interactions in a Dye-lebelled DNA aptamer. *Biophys. J.*, **88**, 3455–3465.
47. Cheng,W., Dumont,S., Tinoco,I. and Bustamante,C. (2007) NS3 helicase actively separates RNA strands and senses sequence barriers ahead of the opening fork. *Proc. Natl. Acad. Sci. U.S.A.*, **104**, 13954–13959.
48. Dumont,S., Cheng,W., Serebrov,V., Beran,R.K., Tinoco,I., Jr, Pyle,A.M. and Bustamante,C. (2006) RNA translocation and unwinding mechanism of HCV NS3 helicase and its coordination by ATP. *Nature*, **439**, 105–108.
49. Wuite,G.J., Smith,S.B., Young,M., Keller,D. and Bustamante,C. (2000) Single-molecule studies of the effect of template tension on T7 DNA polymerase activity. *Nature*, **404**, 103–106.
50. Kaur,P., Plochberger,B., Costa,P., Cope,S.M., Vaiana,S.M. and Lindsay,S. (2012) Hyidrophobicity of methylated DNA as a possible mechanism for gene silencing. *Phys. Biol.*, **9**, 065001.
51. Severin,P.M.D., Zou,X., Gaub,H.E. and Schulten,K. (2011) Cytosine methylation alters DNA mechanical properties. *Nucleic Acids Res.*, **39**, 8740–8751.
52. Severin,P., Ho,D. and Gaub,H.E. (2011) A high-throughput molecular force assay for protein-DNA interactions. *Lab Chip*, **11**, 856–862.
53. Kara,M. and Zacharias,M. (2013) Stabilization of duplex DNA and RNA by dangling ends studied by free energy simulations. *Biopolymers*, **101**, 418–427.